ELSEVIER

Physica A 249 (1998) 1–9

PHYSICA A

Periodic, aperiodic, and transient patterns in vibrated granular layers

Paul B. Umbanhowar [a], Francisco Melo [b], Harry L. Swinney [a,*]

[a] *Center for Nonlinear Dynamics and Department of Physics, The University of Texas at Austin, Austin, TX 78712, USA*

[b] *Departamento de Fisica, Universidad de Santiago, Avenida Ecuador 3493, Casilla 307 Correo 2, Santiago, Chile*

Abstract

Experiments on vertically vibrated granular layers in evacuated containers reveal a variety of patterns for acceleration amplitudes above a critical value ($\approx 2.5\,g$). Stripes, squares, hexagons, spirals, triangles, and targets, as well as particle-like localized excitations ("oscillons") and fronts ("kinks") between regions with different vibrational phase are observed as the layer depth and the container oscillation frequency and amplitude are varied. A zig-zag instability, unstable hexagons, phase-disordered patterns, and "two-phase" squares are also observed. With a few noteworthy exceptions, the patterns are essentially independent of the lateral boundary conditions.

Granular materials are composed of macroscopic particles (grains). Energy is dissipated in each grain collision. The typical energy of a grain is many orders of magnitude greater than $k_B T$, so temperature plays no role in grain dynamics. These two characteristics give granular media properties that differ from those of solids and fluids. Granular media are important in many geological and industrial processes but are much less well understood than solids and fluids. Research in the past decade has revealed a variety of interesting collective phenomena in granular media, e.g. see Ref. [1] and references therein. Here we present observations of spatial patterns in vertically vibrated granular layers.

Our earlier experiments investigated extended standing wave patterns (planar stripes, squares, and hexagons) [2] and localized structures ("oscillons") [3] as a function of the sinusoidal container oscillation frequency f and the dimensionless acceleration amplitude $\Gamma = 4\pi^2 A f^2 g^{-1}$, where A is the amplitude and g the acceleration due to gravity.

* Corresponding author. E-mail: swinney@chaos.ph.utexas.edu.

0378-4371/98/$19.00
PII S0378-4371(97)00425-1

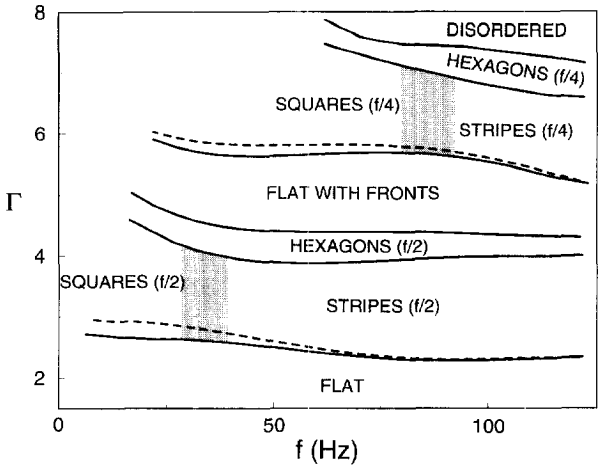

Fig. 1. Stability diagram showing transitions in a 7-particle deep layer. Shaded regions indicate the coexistence of slowly evolving patterns of squares and stripes. Solid (dashed) lines denote transitions with decreasing (increasing) Γ. The transition from a flat layer to square patterns is strongly hysteretic.

In this paper we present aspects of planar patterns and oscillons not presented in the earlier work. A more detailed description of the various phenomena will appear elsewhere [4].

The patterns described here, unless noted otherwise, are produced in a layer of non-cohesive, 0.15–0.18 mm diameter, bronze spheres placed in the bottom of an evacuated, upright, 126 mm diameter, cylindrical container [2,3]. The principal control parameters are the oscillation frequency f (10–120 Hz), Γ (0–10) and the dimensionless layer depth $N = H/D$ (3–30), where H is the layer depth and D the particle diameter. Patterns are visualized by strobed side lighting, and images are acquired with a CCD camera mounted on axis.

Fig. 1 is a phase diagram showing the regions in which different patterns are observed as a function of the container acceleration amplitude and frequency. The effective forcing of the granular layer is different from the container forcing for $\Gamma > 1$ because the layer loses contact with the container when the container acceleration is less than $-g$. The effective forcing magnitude is determined by the collision acceleration, while the effective drive frequency is set by the time between layer–container collisions [2]. Hysteretic subharmonic standing waves arise when the effective forcing magnitude exceeds a critical value ($\Gamma \approx 2.4$). At low f the patterns are squares, while at larger f stripe patterns appear. As Γ is increased past ≈ 4, the layer free-flight time exceeds f^{-1}, at which point there is a doubling of the period in the motion of the layer center of mass: successive free flights last more than a period and less than a period. Hexagonal patterns, which can have two possible phases with respect to the drive signal, arise at this period doubling.

Further increases in Γ reduce both the shorter free flight-time and the effective forcing magnitude until the layer gently collides with the container only once every two

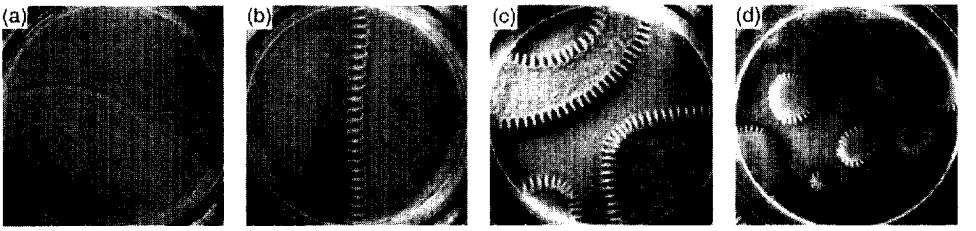

Fig. 2. Fronts between domains with opposite phase in a 7-particle deep layer: (a) $f = 67$ Hz, $\Gamma = 5.8$, (b) $f = 28$ Hz, $\Gamma = 5.2$, (c) $f = 35$ Hz, $\Gamma = 5.1$, and (d) $f = 40$ Hz, $\Gamma = 5.1$. The fronts in (a) and (b) are stationary, while the isolated regions in (d), created by a step change in Γ, shrink and disappear.

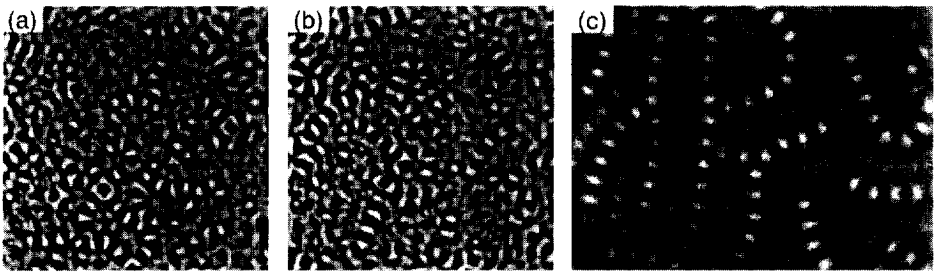

Fig. 3. (a) and (b) Disordered patterns separated in time by 5 s; $f = 70$ Hz, $\Gamma = 8.6$, and $N = 5.3$ (image size, 89×89 m). (c) Pattern in a 0.7 mm deep layer of $D < 0.15$ mm titanium balls, $f = 72$ Hz, and $\Gamma = 8.5$ (image size, 100×75 mm).

container cycles. At this point ($\Gamma \approx 5$) there are no extended wave patterns, just regions with opposite oscillation phase connected by fronts (Fig. 2). The regions with opposite phases collide with the container on alternate cycles, while a front separating these regions collides with the container each cycle and experiences a larger effective forcing than the rest of the layer. At high frequencies the fronts are undecorated (Fig. 2a), while at lower frequencies, a subharmonic standing wave instability develops (Fig. 2b–d). The instability wavelength increases with decreasing f; at very low f the instability vanishes because grains are driven out of the front region due to the violence of the collision. A variety of front shapes are formed by quickly increasing Γ into the front-forming region. A region embedded within another of opposite phase is unstable and shrinks, while fronts which extend to the wall are often stable [5].

As Γ is increased beyond ≈ 5.5, the effective forcing magnitude is large enough so that squares and stripes reappear, as do hexagons at even higher Γ in conjunction with a second-period doubling. This sequence does not continue indefinitely; at $\Gamma \approx 7.8$, the patterns become disordered in both space and time and remain that way for further increases in Γ (Fig. 3). The transition to disorder results from layer/plate collisions that do not occur simultaneously or uniformly in time. With titanium beads, a similar transition occurs but the pattern appears to have less disorder (Fig. 3c).

We now return to the primary bifurcation. At higher frequencies the primary bifurcation is to stripe patterns. Asymptotically, the stripes form locally parallel domains

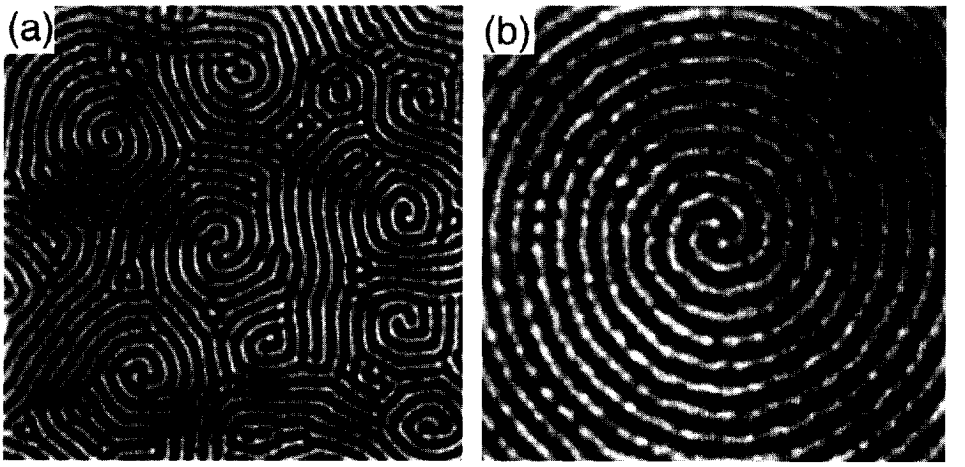

Fig. 4. Spirals (a) at $f = 70$ Hz, $\Gamma = 3.6$, $N = 10$, and $D = 0.07$ mm and (b) with a 2° upward sloping "beach" at $f = 80$ Hz, $\Gamma = 3.6$, and $N = 5$ (images size, 90×90 mm). Pattern (a) evolves to stripes, while (b) evolves from a state similar to (a).

and prefer to align perpendicular to the sidewall. However, at onset, and when the aspect ratio is large, patterns reminiscent of the spiral-defect chaos observed in binary fluid convection arise [6] (Fig. 4a). The granular spirals can be single- or multi-armed and rotate in the direction of chirality. These patterns are transient, eventually being destroyed by the encroachment of stripes growing perpendicular to the wall. However, by adding a "beach" to the perimeter of the container bottom (here the beach is a 2.3 cm wide annular region with a 2° upward slope in a 147 mm diameter container), the orthogonality condition is relaxed and spirals grow until a single large spiral fills the container (Fig. 4b). Like the small spirals, the large spiral rotates in the winding direction and can be multi-armed. The center of the large spiral drifts about and can even "leave" the container.

In layers approximately 15 particles deep or deeper, more patterns arise. Among these are stable localized excitations or "oscillons", which appear for Γ slightly below the value for planar patterns and for f in the vicinity of the square-to-stripe transition [3]. Oscillons are subharmonic: on one cycle they form a peak and on the next a crater. Oscillons of like phase repel while oscillons of opposite phase attract and bind to form more complex structures with coordination number up to three (Fig. 5a–Fig. 5d). When Γ is increased above the upper stability boundary, oscillons grow by nucleating excitations of opposite phase at their outer edges for low f (Fig. 5e), while at higher f, they expand as a domain of growing stripes (Fig. 5f), similar to the transient localized states observed in binary fluid convection [7]. On occasion, an unstable oscillon appears near the wall and forms a chain that grows to encircle the container (Fig. 5g). It appears that sidewall-driven convection reduces the layer depth along the wall, which makes oscillons unstable there (as in Fig. 5e). In the interior, the layer is deep enough so that oscillons are stable and do not grow.

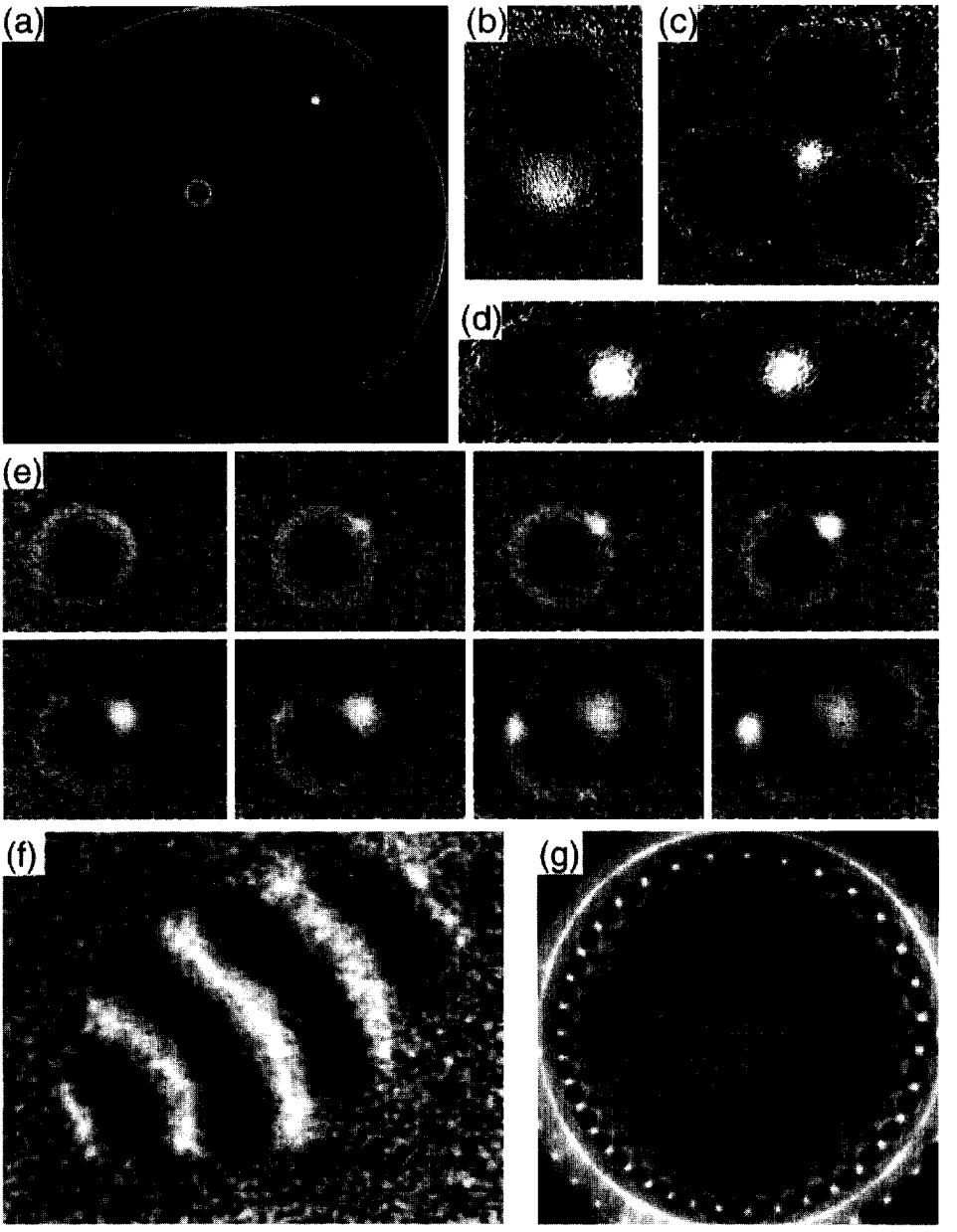

Fig. 5. Oscillons ($N = 17$): (a) isolated crater and peak phases, (b) dipole, (c) tetramer, (d) chain, (e) evolution for Γ above upper stability limit at $f = 24$ Hz (elapsed time between images is $\approx 10 f^{-1}$), (f) snapshot of evolution for Γ above upper stability limit at $f = 31$ Hz, and (g) ring. In (a)–(d) and (g), $f = 26$ Hz and $\Gamma = 2.45$. The oscillon diameter is 5 mm in (a) (d) and (g), and 6 mm in (e) and the wavelength is 7 mm in f.

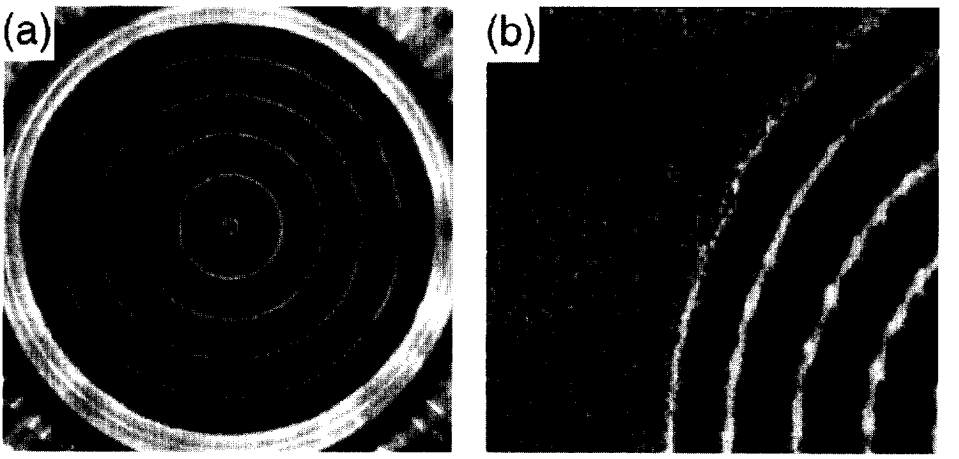

Fig. 6. (a) Stable target pattern ($f = 28$ Hz, $\Gamma \approx 3$, and $N = 17$) and (b) waves nucleated at a point along the wall, spreading into flat region ($f = 26$ Hz, $\Gamma \approx 3$, and $N \approx 20$). (b) image size is 80×80 mm.

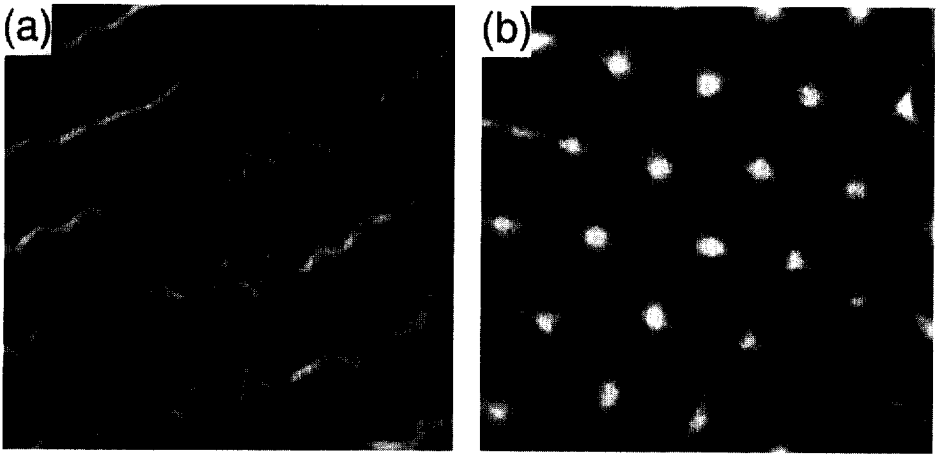

Fig. 7. (a) $f/4$ instability of stripe patterns ($f = 23$ Hz, $\Gamma = 3.0$, and $N = 18$) and (b) unstable hexagons in square regime, 1% above onset ($f = 24$ Hz, $\Gamma = 2.4$, and $N \approx 20$). Image sizes are 60×60 mm.

Another phenomenon, also related to sidewall friction, is the target pattern (Fig. 6a). Targets are formed by stepping Γ from below onset to a value within the hysteretic region for f in the stripe regime. Waves are nucleated at the wall and travel inward. (Fig. 6b shows a wave nucleated at a point along the wall spreading into the container interior.) If the nucleation occurs uniformly, a target is formed; otherwise, spiral or disordered patterns result. Although stable target patterns are observed, they usually decay via the introduction of defects at the wall, which travel to the center and create a spiral. Spirals accumulate more arms with the introduction of further defects until they break up and form a stripe pattern. We speculate that targets, once they are formed, are stable if the container radius is an integral number of wavelengths.

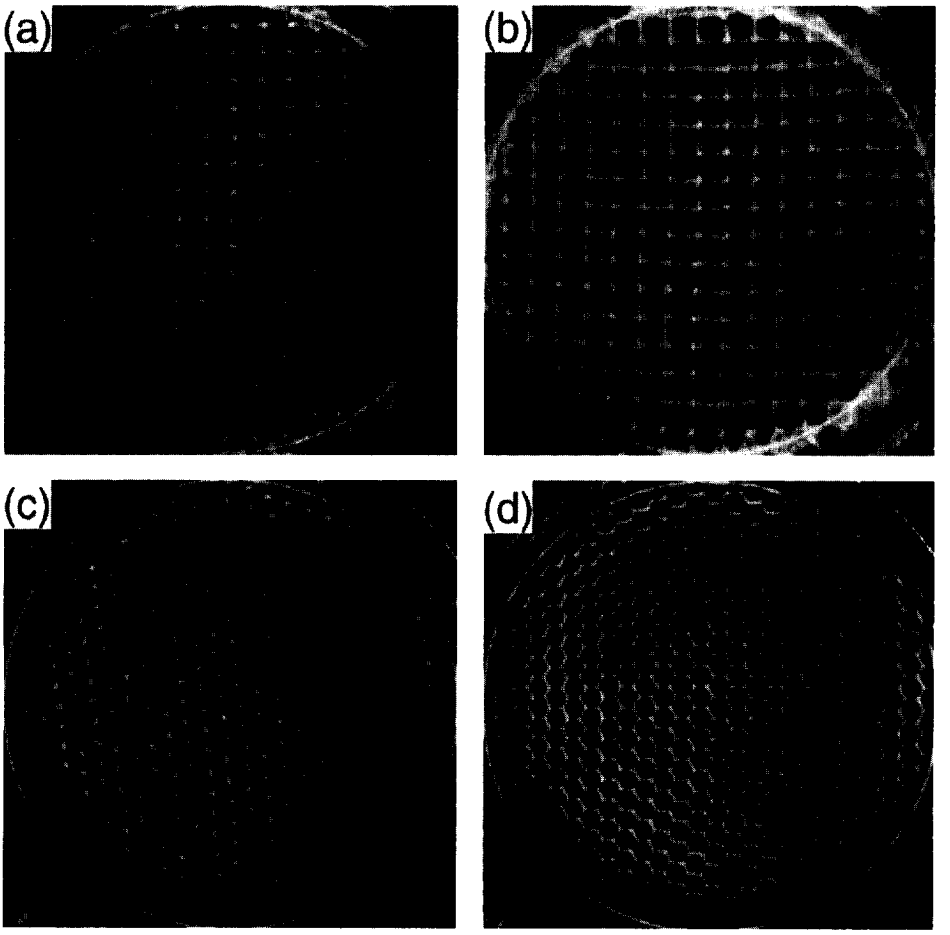

Fig. 8. Two-phase squares with single-frequency forcing, (a) peak phase and (b) cellular phase ($f = 17$ Hz, $\Gamma = 2.5$, and $N = 12$); these uniform phase patterns are atypical – domains with opposite phase are usually present simultaneously (note, row of peaks at bottom of (b)). Hexagons with two-frequency forcing $A_1 \sin 2\pi f t + A_2 \cos \pi f t$, (c) peak phase and (d) cellular phase ($f = 32$ Hz, $\Gamma = 2.8$, $A_2 = 0.1A_1$, and $N = 5.3$).

Other phenomena, in addition to targets and oscillons, are also observed in deep layers ($N \geqslant 15$). For f near the square/stripe transition region, a lateral zig-zag instability of the stripe pattern occurs (Fig. 7a). Zig-zags oscillate at $f/4$ and grow during layer free flight; at low f and large Γ, the transverse oscillation amplitude is about as large as the pattern wavelength. Another pattern, unstable hexagons, occurs close to the lower stability boundary ($\Gamma \approx 2.4$) for f in the square regime (Fig. 7b). Patches of hexagons are typically 2–4 wavelengths wide and persist for about $100\,f^{-1}$ before reverting to squares.

Another phenomenon, perhaps related to transient hexagons, is a regime with squares with two distinct phases, as shown in Fig. 8a and Fig. 8b. Unlike normal squares, which

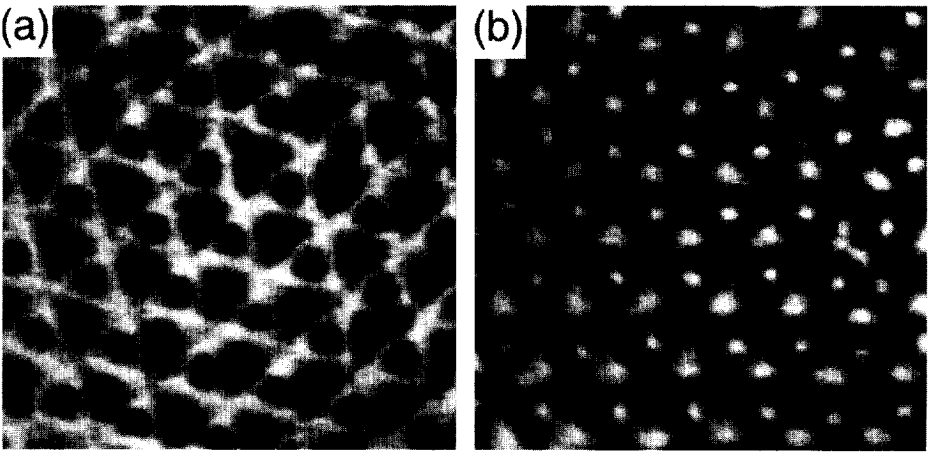

Fig. 9. (a) and (b) Two phases of triangular patterns obtained by alternately forcing with $\sin\phi \sin 2\pi f_1 t$ for 5 cycles and $\cos\phi \sin 2\pi f_2 t$ for 4 cycles ($f_1 = 37.5$ Hz, $f_2 = 30$ Hz, $\phi = 60°$, $\Gamma = 3.8$, and $N = 13$). Images are 60×60 mm. Pattern has rotated between (a) and (b).

have the same profile from cycle to cycle, two-phase squares resemble hexagons (Fig. 8c and Fig. 8d): on one cycle the pattern is cellular, while on the next a lattice of peaks. Two-phase squares arise near onset. Typically, both peak and cellular square phases exist simultaneously in different spatial domains, but a single phase, as shown in Fig. 8a and Fig. 8b can persist for hundreds of cycles.

The hexagons that form at $\Gamma \approx 4$ arise from an intrinsic two-frequency forcing at f and $f/2$, which, as described, arises from a period doubling of the oscillating layer. Two-frequency forcing of the container itself can also produce hexagons, as Fig. 8c and Fig. 8d illustrates; unlike the hexagons produced by period doubling, the hexagons in Fig. 8c and Fig. 8d do not have the phase degeneracy that leads to fronts between domains of different phase.

Driving the container with more complicated waveforms can lead to other patterns. For example, forcing with composed sinusoids at f and $\frac{4}{5}f$ produces a triangular pattern (Fig. 9). We have not yet, however, observed quasi-patterns like those found with multi-frequency driving of viscous fluids [8].

The variety of patterns observed in vibrated granular layers provides a challenge to theory. Any theory that can reproduce these patterns (e.g. Ref. [9]) should yield new general insights into the dynamics of granular media.

Acknowledgements

This research was supported by the US Department of Energy Office of Basic Energy Sciences, the Texas Advanced Research Program, the US National Science Foundation Division of International Programs, and Fondecyt (Chile).

References

[1] H.M. Jaeger, S.R. Nagel, R.P. Behringer, Rev. Mod. Phys. 68 (1996) 1259.
[2] F. Melo, P.B. Umbanhowar, H.L. Swinney, Phys. Rev. Lett. 75 (1995) 3838.
[3] P.B. Umbanhowar, F. Melo, H.L. Swinney, Nature 382 (1996) 793.
[4] P.B. Umbanhowar, F. Melo, H.L. Swinney, 1997, to be published.
[5] L. Caballero, P.B. Umbanhowar, F. Melo, 1997, to be published.
[6] S.W. Morris, E. Bodenschatz, D.S. Cannell, G. Ahlers, Phys. Rev. Lett. 71 (1993) 2026.
[7] K. Lerman, E. Bodenschatz, D.S. Cannell, G. Ahlers, Phys. Rev. Lett. 70 (1993) 3572.
[8] W.S. Edwards, S. Fauve, J. Fluid Mech. 278 (1994) 123.
[9] L.S. Tsimring, I.S. Aranson, Phys. Rev. Lett. 79 (1997) 213.